Tonkul *et al. Geothermal Energy* (2026) 14:2
https://doi.org/10.1186/s40517-025-00372-3

Geothermal Energy

RESEARCH Open Access

Fluid–CO_2 injection in a hypersaline volcanic systems: a reactive transport and experimental evaluation with application to the Tuzla Geothermal Field, Türkiye

Serhat Tonkul[1,2*], Selçuk Erol[3], Alper Baba[4] and Simona Regenspurg[5]

*Correspondence:
s.tonkul-1@tudelft.nl

[1] Department of Environmental Engineering, İzmir Institute of Technology, 35430 Urla, İzmir, Türkiye
[2] Faculty of Civil Engineering and Geosciences, Reservoir Engineering, Delft University of Technology, Stevinweg 1, 2628CN, Delft, The Netherlands
[3] Department of Petroleum and Natural Gas Engineering, Middle East Technical University, 06800 Ankara, Türkiye
[4] Department of International Water Resources, İzmir Institute of Technology, 35430 Urla, İzmir, Türkiye
[5] Helmholtz-Zentrum Potsdam, Deutsches GeoForschungsZentrum GFZ, Potsdam, Germany

Abstract

This study evaluates the CO_2 sequestration capability of the Tuzla Geothermal Field (TGF) in northwest Türkiye under reservoir conditions (200 °C and 4.4 MPa). While ongoing studies at TGF have investigated CO_2 co-injection primarily for geothermal heat extraction, the present study focuses on the associated potential for long-term CO_2 storage. To this end, CO_2–brine–rock interactions were examined through batch reactor experiments and reaction path modeling using the PhreeqC geochemical tool. The experiments revealed complex dissolution/precipitation reactions that altered reservoir properties, with mineralogical analyses (XRD, XRF, SEM, and EDS) showing the formation of secondary phases such as calcite, kaolinite, and Ca-rich aluminosilicates. These results indicate that the Tuzla reservoir rocks provide sufficient divalent cations to support mineral trapping under reservoir conditions. Overall, our findings highlight that, in addition to its promise for heat extraction, CO_2 co-injection at TGF offers an opportunity for permanent geological storage, thereby strengthening the dual benefits of this approach.

Keywords: CO_2 sequestration, Saline systems, High enthalpy, Tuzla, PhreeqC, Reactive transport modeling

Introduction

Greenhouse gas (GHGs) emissions to the environment have grown in importance in industrial processes in recent years (Junior et al. 2025). In particular, the primary contributor to global warming is carbon dioxide (CO_2), which accounts for about 80% of GHGs. Moreover, global warming caused by anthropogenic activity has increased by 1.0 °C over pre-industrial levels and is predicted to reach 1.5 °C by 2030 (Fawzy et al. 2020). One of the most effective and sustainable strategies for reducing CO_2 emissions is to capture the CO_2 from facilities and sequestrate it in geological media (Aradóttir et al. 2012; Clark et al. 2020; Snæbjörnsdóttir et al. 2014). It is possible to trap the injected CO_2 inside the geological formation through physical and geochemical trapping (Bachu et al. 2007). The integrity of the cap rock controls physical trapping, which typically

© The Author(s) 2026. **Open Access** This article is licensed under a Creative Commons Attribution 4.0 International License, which permits use, sharing, adaptation, distribution and reproduction in any medium or format, as long as you give appropriate credit to the original author(s) and the source, provide a link to the Creative Commons licence, and indicate if changes were made. The images or other third party material in this article are included in the article's Creative Commons licence, unless indicated otherwise in a credit line to the material. If material is not included in the article's Creative Commons licence and your intended use is not permitted by statutory regulation or exceeds the permitted use, you will need to obtain permission directly from the copyright holder. To view a copy of this licence, visit http://creativecommons.org/licenses/by/4.0/.

Springer

happens shortly following injection. On the other hand, the chemistry of the brine and the rock determines geochemical trapping, which often occurs while the CO_2–water–rock interaction continues after injection (Steel et al. 2018; Liu et al. 2019). Geochemical trapping can be divided into solubility trapping and mineral trapping. Solubility trapping is the process in which injected CO_2 dissolves into water and permanently turns the aqueous phase (Liu et al. 2019). Subsequently, acidity in subsurface geological formations is increased by CO_2 dissolution in water. Consequently, a number of the host rocks' main minerals dissolve into the formation water at low pH levels. The concentrations of metal divalent cations such as Ca^{2+}, Mg^{2+}, and Fe^{2+} increase to form carbonate minerals under these circumstances. This phenomenon is known as mineral trapping (Saadatpoor et al. 2010).

Over the past 30 years, a number of geochemists have developed a number of experiments under various conditions to measure the mineral kinetic rates (Burch et al. 1993; Fu et al. 2009; Gautier et al. 1994; Hellmann 1994; Lu et al. 2015; Nagy and Lasaga 1992; Oelkers et al. 1994). They all concurred that experimental methods under dynamic and stable chemical circumstances should be used to evaluate mineral kinetic rates. On the other hand, extensive research has been carried out on CO_2 sequestration experimentally, numerically, or in actual field studies (Akın et al. 2025; Berndsen et al. 2024; Erol et al. 2022; Kaya and Zarrouk 2017; Kolditz et al. 2012). Ajayi et al. (2019) conducted a comprehensive analysis of the operational concepts and significance of underground CO_2 sequestration. The expected outcomes of the study are a synthesis of the current status of CO_2 geological storage, an analysis of capture mechanisms and migration processes, a comparative assessment of modeling approaches for storage capacity estimation, a review of monitoring and verification techniques, and identification of key technical challenges and future research directions. Addassi et al. (2022) investigated the feasibility of injecting carbonated water into unconfined aquifers as a long-term CO_2 storage method. The study focuses specifically on a geothermal reservoir, systematically explores a wide range of hydrogeological and geochemical parameters, and quantitatively evaluates the water-to-CO_2 ratios and density conditions required to ensure secure solubility trapping, thereby extending the applicability of carbonate water injection beyond the scope of previous works. Their results suggested that CO_2 may be securely stored using solubility trapping. For the CarbFix project at Hellisheidi, southwest Iceland, Aradóttir et al. (2012) evaluated the CO_2–fluid–rock interaction. Their goal is to determine whether in situ CO_2 mineral sequestration in Iceland's basaltic rocks is feasible. After mixing the captured CO_2 with the effluent fluid, it is subsequently injected into a geothermal reservoir. In this procedure, solubility trapping is used to first trap the injected CO_2. Once the injected CO_2 has mixed with the formation fluid, it may then generate bicarbonate and carbonic acid. In the process, the injected CO_2 diffuses, combines with the formation fluid, and mostly changes into bicarbonate and carbonic acid, two other aqueous species. Complex chemical processes that result in the immobilization of CO_2 can be triggered by the dissociation of bicarbonate and carbonic acid ions. CO_2 is then trapped in solid mineral phases, such as calcite and dolomite (Matter et al. 2016; Přikryl et al. 2018). Wan et al. (2016) used TOUGHREACT to evaluate reactive transport processes in the reservoir and assess the geochemical reaction impact on the changes in permeability and porosity of CO_2-EGS in the geothermal site at Desert Peak

(Nevada). The main minerals undergoing dissolution, according to modeling studies, are quartz, chlorite, albite, anorthite, and K-feldspar. The following are the main secondary minerals that precipitate: siderite, calcite, kaolinite, illite, smectite, and dolomite. To analyze fluid–rock interactions throughout the flow pathways connecting the injection and production wells of the Nesjavellir geothermal reservoir, Galeczka et al. (2022) used reaction path modeling. As the fluid moves further into the reservoir from the injection well, the geofluid temperature increases from 84 to 300 °C. The authors calculate that 70% of the injected CO_2 can mineralize along the flow pathway based on their geochemical modeling results. Erol et al. (2022) used TOUGHREACT to model a possible fluid–CO_2 injection into deep metamorphic formation rocks consisting of quartzite, schist, and marble in the Kızıldere geothermal field in Türkiye. They created three different scenarios, including three annual injection rates of CO_2 for 10 years. The two main objectives of their study are: (i) to identify the mineralization process and (ii) to assess the dynamic fluid–rock interactions with the highest feasible CO_2-charged fluid input. The solubility of CO_2 in the effluent fluid was less than 0.1 mol/kg, and the partial pressure of CO_2 near the pilot injection well was less than 1 MPa during the injection. According to their modeling results, under all conditions, the maximum CO_2-charged fluid mixture is stable in a single phase. They concluded that the distinct mineral compositions of the metamorphic rocks are under consideration and the variations in the CO_2 mass fraction of the injected fluid and the reservoir restrict the process of CO_2 mineralization.

Field studies on CO_2 co-injection are successfully carried out using industrial CO_2 to reduce scale (mineral precipitation) problems in the borehole and surface installations in the TGF, so in this respect, it is a pilot field in Türkiye (Topcu et al. 2019). However, the geochemical reactions between reservoir rock, fluid, and CO_2 have yet to be understood for the TGF. To address this research gap, we conducted a batch reaction experiment and a geochemical model to confirm the feasibility of CO_2 sequestration. The study focuses on analytical, experimental, and geochemical modeling methods.

The main intention of this study is to:

- reveal whether the TGF reservoir is suitable for CO_2 sequestration, and
- provide a basis for extending the CO_2 co-injection study currently used in the TGF to CO_2 sequestration.

CO_2 co-injection in the TGF

The TGF is an active tectonic field located 5 km from the Aegean Sea in Türkiye and 80 km south of Çanakkale (Fig. 1). The reservoir rocks of the TGF consist of Miocene-aged volcanic rocks, which are mainly andesite/trachyandesite. The cap rocks in the system are composed of Neogene-aged claystone and sandstone (Karamanderesi 1986; Mützenberg 1990; Samilgil 1966; Şener and Gevrek 2000). Hydrothermal activity and the active thermal regime in the region have continued since Miocene volcanism.

Injecting industrial CO_2 into the geothermal system to prevent the scale formation in the TGF has been applied by Topcu et al. (2019) (Fig. 2a). A CO_2 mobile heating tank, a static mixer, a check valve, a flow meter, a solenoid valve, a regulator, a safety valve, a pH meter, and a flow meter are used to inject industrial CO_2 into the system (Fig. 2b). The

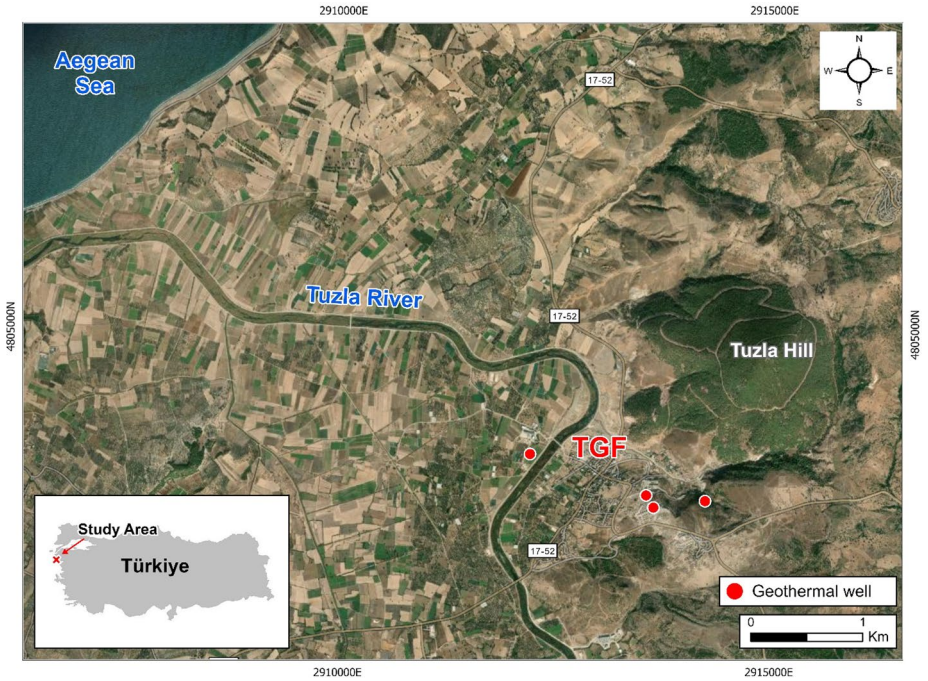


Fig. 1 The TGF and its surrounding area

mobile heater tank contains CO_2 in liquid. Thus, the mobile tank heater is used to heat CO_2 before it is transferred to the dosing system. The system, which is designed to use a static mixer, is used to create a homogeneous mixture of brine and CO_2 (gas). Following the separators, a static mixer with a CO_2 diffuser is added to the brine pumps' outlet. After regulating the pressure and gasifying the liquid CO_2 in the evaporator, it is transferred to the static mixer to mix with brine. For operational safety, a check valve is added to the system after the CO_2 (gas) dosing point. Monitoring the volumetric flow rate of CO_2 (gas) is done with a flow meter connected to the system. The safety valve maintains the pressure below 25 bar, while the regulator permits the CO_2 (gas) pressure to surpass the brine pressure. With the aid of the pH probe, a series of samples is periodically collected from the measurement point after the pump.

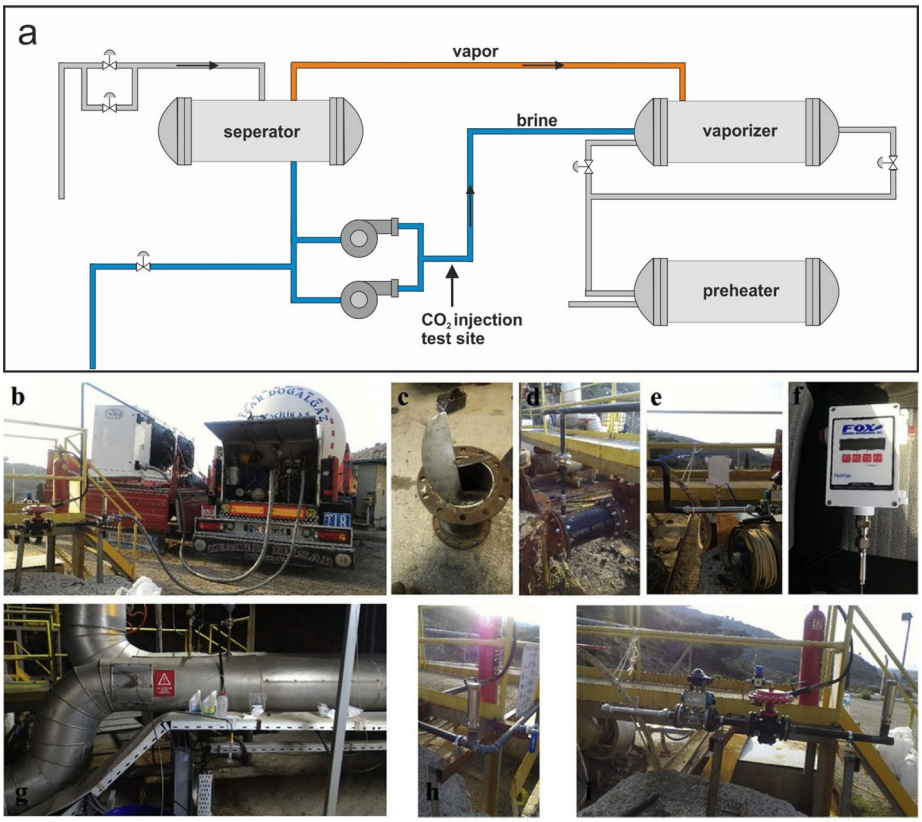
Currently, field studies are successfully carried out using industrial CO_2 to reduce scale (mineral precipitation) problems in the TGF. Now, field engineers are searching for answers to extend the CO_2 co-injection study to CO_2 sequestration. CO_2 sequestration study in the TGF is discussed in detail in the following sections.

Materials and methods

A flowchart of experimental, analytical, and geochemical modeling processes is given in Fig. 3.

Experimental setup

A high-pressure batch reactor has been utilized to conduct a series of CO_2–fluid rock dissolution/precipitation reactions using reservoir rock samples. The brine sample is collected from a production well in the TGF, and andesite, the primary volcanic host



a) Binary system of the TGF, b) mobile heater tank, c) static mixer, d) check valve, e-f) flow meter, g) pH meter, h) safety valve, i) solenoid valve.

Fig. 2 CO_2 co-injection study in the TGF (Topcu et al. 2019)

rock of the reservoir, is used in the study. Six grams of sieved rock powder and 60 mL of reservoir fluid were used. The rock sample was crushed to grain sizes smaller than 125 μm to improve the XRD analysis. The rock sample had particles ranging in size from sub-micron to micron prior to the batch reaction experiment. First, analytical-grade acetone was used to clean these particles, and afterward deionized water was used to rinse them. Prior to the batch reactor experiment, the material was dried overnight at 105 °C.

The 100-mL batch reactor (BERGHOF instrument) utilized in this investigation provides the highest level of safety up to 20 MPa and 300 °C. Figure 4 shows a schematic illustration of the experimental setup. The reactor has three ports for fluid sampling, gas injection, and gas sampling. A thermometer and a barometer are also included with the reactor. First, the pressure inside the vessel was adjusted, and the sampling line was purged by connecting a CO_2 gas tank to a pressure regulator. Later, a nitrogen (N_2) gas line is connected to the sampling valve to remove oxygen from the brine. Removing oxygen from the brine in a batch reaction experiment is important as Fe-bearing phases will react differently if the brine contains oxygen. After the vessel had been filled and sealed, the temperature was raised to the desired target value of 200 °C. To prevent boiling when heating to the desired reaction temperature, a

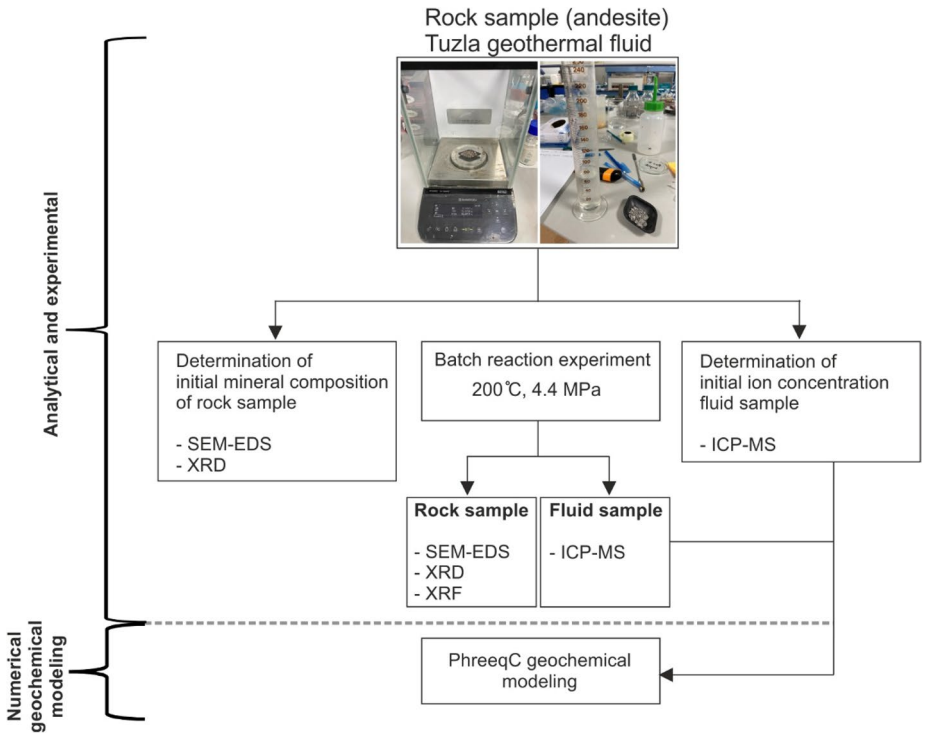
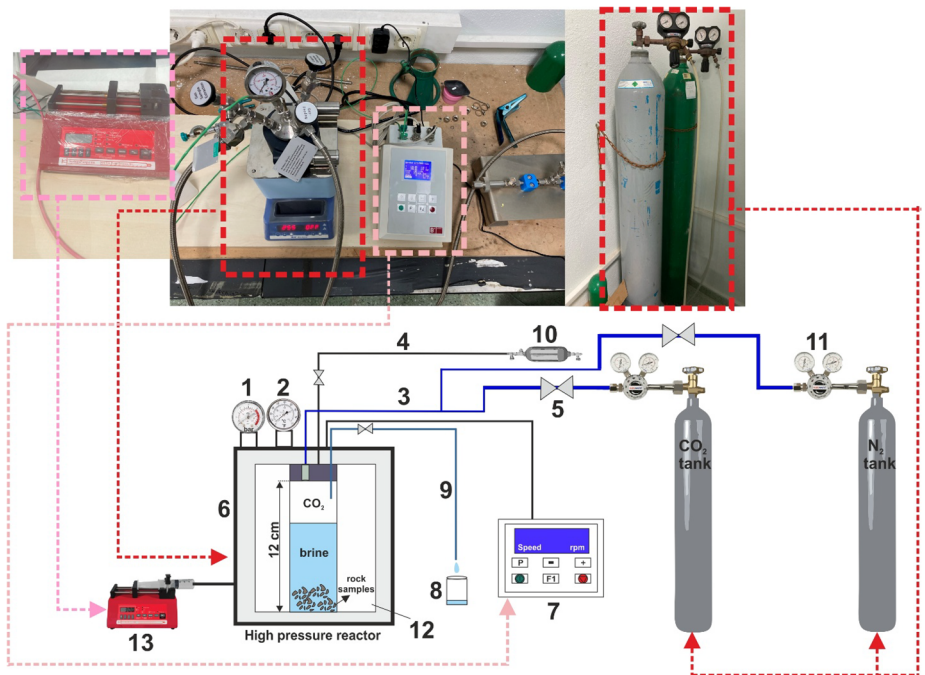


Fig. 3 Flowchart of analytical, experimental, and geochemical modeling process



1-Barometer, 2-Thermometer, 3-Gas injection line, 4-Gas sampling line, 5-Valve, 6-Heating jacket
7-Data acquisition system, 8-Fluid collection bottle, 9-Fluid collection line, 10-Gas collection bottle
11-Pressure regulator, 12-Reactor, 13-Syringe pump

Fig. 4 Schematic representation of the experimental setup

total pressure was applied as 4.4 MPa. According to Tödheide and Franck (1963), the partial pressure of CO_2 in the reaction vessel was determined to be 2.27 MPa. In situ conditions were used to inject 0.167 mol/kgw CO_2 at a steady flow rate of 0.1 mL/min into the brine (11.72 mol NaCl). The reactor temperature reached 100 °C in approximately 5–10 min and 200 °C in 40–45 min. Fluid samples were collected every 3 days during the 9-day trial. These intervals correlated to 72, 144, and 216 h following CO_2 injection. Throughout the experiment, three fluid samples were collected. In the meantime, the fluid sample instrument was kept from clogging by using a micromesh stainless steel wire basket.

Analytical calculations

Experimental fluid samples were analyzed for major and minor components using ICP-MS (Inductively Coupled Plasma Mass Spectrometry, Agilent 7500ce) with a simultaneous analog and pulse counting detector. NIST-traceable single or multi-element standard solutions were used to calibrate the system. The mean and standard deviation for each chosen elemental mass were calculated by repeating standards and blanks five times for each sample. Using an Accumet AR-20 m and a THERMO combination glass pH/reference electrode, the pH of each fluid sample was measured under standard laboratory conditions. The initial and final brine compositions are given in Table 1. The mineralogical alterations were characterized using X-ray diffractometer (XRD), X-ray fluorescence (XRF), scanning electron microscopy (SEM), and diffraction spectrometer (EDS) both before and after the experiment. The rock sample was analyzed using SEM and EDS in FEI Quanta 250 FEG to visualize at the micro-scale. The elemental content of the rock structure was ascertained both quantitatively and subjectively using the EDS detector, and mapping was used to monitor the distribution of the elements on the image. The XRD and XRF analyses of the rock sample were assessed utilizing the Philips X'Pert Pro and the Spectro IQ II, respectively. XRD provides information on the material's crystal size, non-crystalline phase content, and phase concentration.

Numerical geochemical modeling

The experiment in this study was numerically simulated using the PhreeqC 3.7.3 geochemical modeling tool together with the LLNL database (Parkhurst and Appelo 1999; Wolery and Daveler 1992). Henry's Law was used to calculate the solubility of CO_2 based

Table 1 The initial composition of the geothermal fluid and the changes of major composition in the brine

	Elements (mg/l)										
	Ca^{2+}	Na^{+}	K^{+}	Mg^{2+}	SiO_2	Al^{3+}	Fe^{3+}	Cl^{-}	Ca/Na	Ca/Si	Mg/Ca
Initial brine composition	3090.00	18001.00	1809.19	131.00	189.00	4.78	5.49	34560	0.1717	16.3492	0.0424
Reaction time (h)											
72	2981.85	18411.87	1837.12	144.38	210.01	2.20	6.22	35300	0.1620	14.1986	0.0484
144	2970.15	18449.46	1841.57	172.04	159.65	2.00	6.48	33252	0.1610	18.6041	0.0579
216	2971.90	18473.12	1841.00	175.23	150.24	2.00	6.42	34365	0.1609	19.7810	0.0590

on the approach of Lichtner et al. (2003). Palandri and Kharaka (2004) stated that the kinetic reaction rate constant (k) changes with temperature. However, the rate constants are mainly evaluated for a pure phase mineral and a strictly regulated pH buffer solution typically used in experiments to determine dissolution rates; ideally, these experiments cover a broad range of pressure, temperature, and pH levels. When the rate constants are applied to intricate natural systems, an adjustment for the rate constants is required to expand the significance of more complex systems (Berndsen et al. 2024). The kinetic reaction path modeling method can be used to fit the results of the batch reactor experiment to acquire new kinetic rate constants of minerals.

Kinetic rates

Transition state theory (TST), as implemented in PhreeqC, was used to determine all mineral reaction dynamics in this study. Equation (1) shows how the TST rate law links the rates of mineral dissolution to the corresponding reactive surface area (A_m), reaction rate constant (k_m), and the thermodynamic driving force of the reaction ($f(\Delta G)$) (Aagaard and Helgeson 1982; Lasaga 1981; Steefel et al. 2015):

$$R_m = A_m \cdot k_m \cdot f(\Delta G). \tag{1}$$

Due to variations in reaction dependencies, such as pH sensitivity, individual mineral dissolving rates vary even when the precise rate law was applied to all mineral phases. While parallel rate laws consider pH dependencies, PhreeqC uses the Arrhenius equation to adapt mineral reaction rates to temperature. In PhreeqC, the rates at which minerals dissolve change with pH. Depending on the mineral phase, acidic and alkaline dissolution processes follow distinct reaction paths. Following the procedure described in Beckingham et al. (2016), mineral rate constants were interpolated from literature data and modified based on formation temperature and expected acidic pH conditions. In general, different studies have different kinetic rate constants. Numerous variables, including experimental design, sample preparation, and mineral composition, may contribute to this difference. pH-related changes in rate constants are usually 1 or 2 orders of magnitude, while other changes are usually considerably less noticeable (Haase et al. 2016). The mineral kinetic rates used for this study are given in Table 2.

Mineral surface area

The effective total area of the solid–liquid interface is referred to as a mineral-reactive surface area. Reactive surface area is a significant source of uncertainty (Dethlefsen et al. 2012) but a crucial parameter, particularly for accurate dissolution experiment interpretation (Luo et al. 2012). In natural geologic samples, mineral-reactive surface areas are typically poorly restricted (Luhmann et al. 2014) and may not be similar to surface areas measured in lab samples (Li et al. 2014). However, the reactive surface areas of natural samples need to be known to simulate kinetically controlled mineral–fluid reactions. The reactive surface area can be obtained in two different methods. The first uses the gas sorption (B.E.T.) method (Brunauer et al. 1938), whereas the second uses straightforward geometric calculations (White and Peterson 1990). In this study, we used geometric calculation to obtain mineral surface areas. Kieffer et al. (1999) stated that simple geometric calculations can be used to calculate the reactive surface areas of the minerals.

Table 2 An overview of the variables that characterize the kinetic reaction rates of the minerals utilized in the models

Minerals	Calculated best-fit rate constants for this study (mol m^{-2} s^{-1})	Grain size (μm)[b]	Surface area (m^2 g^{-1})[b,d]	Calculated surface area (m^2 g^{-1})[c]	Acid[a]		*n*	Neutral[a]		Base and carbonate[a]		*n*
					k_{25} (mol m^{-2} s^{-1})	E (J mol^{-1})		k_{25} (mol m^{-2} s^{-1})	E (J mol^{-1})	k_{25} (mol m^{-2} s^{-1})	E (J mol^{-1})	
Kaolinite[a]	4.2×10^{-11}	5–100	13.2	11.023	4.90×10^{-12}	65900	0.777	6.61×10^{-14}	22200	8.91×10^{-18}	17900	−0.472
Quartz[a]	1.95×10^{-13}	75–125	0.111	0.022	–	45600	–	3.98×10^{-14}	90900	–	–	–
Albite[a]	2.75×10^{-8}	75–150	0.164	0.148	6.92×10^{-11}	65000	0.457	2.75×10^{-13}	69800	–	–	–
Muscovite[a]	3.8×10^{-7}	10–250	0.015[d]	0.021	1.41×10^{-12}	22000	0.370	2.82×10^{-14}	22000	2.82×10^{-15}	22000	−0.220
Hematite[a]	3.1×10^{-14}	50–100	1.11	0.911	4.07×10^{-10}	66200	1.000	2.51×10^{-15}	66200	–	–	–
Calcite[a]	2.51×10^{-4}	44–81	0.021	0.016	5.01×10^{-1}	14400	1.000	1.54×10^{-6}	23500	3.31×10^{-4}	35400	1.000
Biotite[a]	3.0×10^{-9}	10–125	4.74	3.819	1.44×10^{-10}	22000	0.525	2.81×10^{-13}	22000	–	–	–

In the table, the specific surface areas are not provided by Beckingham et al. (2016)

[a] Palandri and Kharaka (2004)

[b] Beckingham et al. (2016)

[c] calculated based on the grain size of minerals and assuming the grains have spherical shape

[d] From Carbfix_kin.dat database (Heřmanská et al. 2020)

Notation: k: kinetic rate constant; E: Activation energy; *n*: Reaction order

By assuming that every mineral grain has the same grain size (< 125 μm), this method allows the predicted surface areas of mineral grains to be derived. However, the mineral grain form is asymmetrical in nature. The surface area of minerals is not accurately estimated because of these imperfections. A surface roughness factor (RF) is used in the calculation to correct for these imperfections (Anbeek 1992):

$$GSA = \frac{4\pi r^2}{\frac{4}{3}\pi r^3 \rho} \tag{2}$$

$$SSA = GSA \times RF. \tag{3}$$

In Eq. 2, r is the radius of mineral grain size (m), ρ is the density of mineral (g m^{-3}). Geometric surface area (GSA) can be calculated by simply dividing the total surface area of the mineral by the particle mass (Eq. 2). Later, GSA is multiplied by the roughness factor (RF) to obtain the mineral specific surface area. According to Hodson (1998), the RF varies between 1 and 20 for feldspar minerals. On the other hand, Holdren and Speyer (1987) reported that the RF changes from 3 to 14 for unweathered alkali feldspars. Determination of the surface area of the reacting minerals is particularly difficult when pore space and mineral heterogeneity are taken into account. Consequently, Table 2 provides the calculated surface areas for each mineral employed in simulations together with their literature values taken from Beckingham et al. (2016).

Results and discussion

Fluid chemistry during reaction

The fundamental factor starting the geochemical reactions is the dissolution of CO_2 in the brine. It dissolves in the brine and mostly forms HCO_3^-. Following the CO_2 injection, the pH of the system decreased from 5.6 to 5.01, which is due to the acidic nature of CO_2 (Fig. 5). The fluctuations in pH can be attributed to interactions and chemical

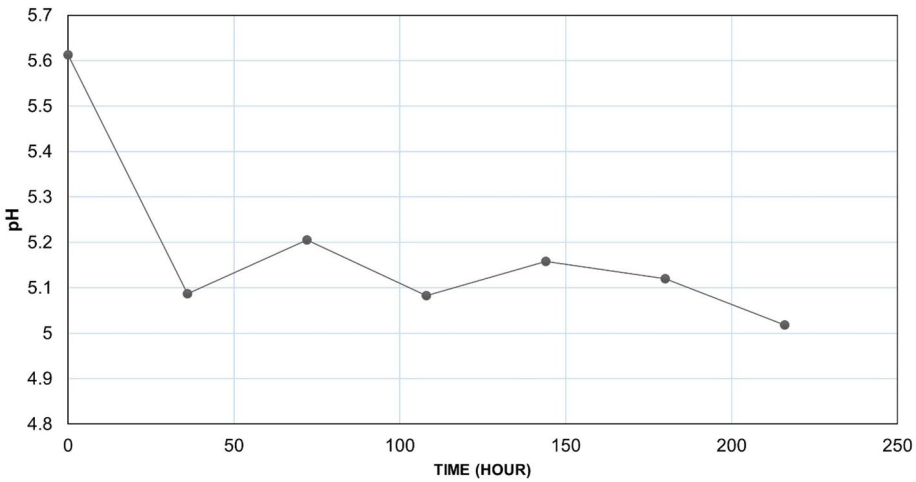


Fig. 5 Changes in the pH of the brine during CO_2 injection

equilibrium between the gas (CO_2), the geothermal fluid, and the rock samples. After CO_2 injection, rapid CO_2 dissolution decreased the pH. Over time, carbonate dissolution, mineral buffering reactions, such as dissolution/precipitation of carbonates and silicates, and ion-exchange reactions moderated the acidity, leading to slight increases in pH at some points.

These reactions are illustrated in Eqs. 4 and 5:

$$CO_2 + H_2O \rightarrow H^+ + HCO_3^- \tag{4}$$

$$HCO_3^- + Ca^{2+} \rightarrow CaCO_3(Calcite) + H^+ \tag{5}$$

Time series changes in fluid chemistry are listed in Table 1 and illustrated in Fig. 6. The majority of geological chemists have indicated that pH is an important factor in the mineral dissolution and precipitation processes (Luo et al. 2001; Oelkers et al. 1994; Wild et al. 2016).

The concentration of SiO_2, Na^+, Ca^{2+}, and Al^{3+} in the brine changed significantly with the continuous dissolution reactions of alkaline feldspar. The initial concentration of SiO_2 is measured as 189 mg/l in the brine. After 72 h of reaction, dissolved SiO_2 gradually ascended to 210.01 mg/l. Afterward, it dropped to 159.65 mg/l over the next 144 h of response and then continued to decrease to 150.24 mg/l at the end of the experiment. This is most likely because, in accordance with Eq. 6, albite releases SiO_2 and Na^+ ions into the brine while consuming H^+ during dissolution during the first 72 h (Fig. 6a and b).

$$NaAlSi_3O_8(Albite) + H^+ = AlO(OH)(Boehmite) + Na^+ + 3SiO_{2(aq)} \tag{6}$$

As the reaction proceeds, compositional changes in the brine indicate that albite is continuously dissolved after 72 h, replacing boehmite with kaolinite. The following reaction explains this phenomenon (Eq. 7):

$$AlO(OH)(Boehmite) + 0.5H_2O + SiO_{2(aq)} = 0.5Al_2Si_2(OH)_4(Kaolinite) \tag{7}$$

The experiment shows evidence for boehmite conversion to kaolinite as indicated by the decrease in dissolved SiO_2 concentration (Fig. 6a). In our observations, we can easily understand that albite first starts to dissolve by releasing SiO_2 into the brine to form boehmite after CO_2 injection and then the excess SiO_2 is consumed by boehmite to form kaolinite. The SiO_2 concentration is measured as 150.24 mg/l at the time of 216 h. The results of the PhreeqC simulation indicate that boehmite precipitation occurs; however, the XRD and SEM analyses do not reveal trace amounts of boehmite. The behavior of albite in our experiment is consistent with its disintegration under comparable experimental conditions, as described by Hellmann (1994).

The amount of Na^+ in the fluid increased significantly and steadily during the experiment (Fig. 6b). The initial concentration of Na^+ is 18001 mg/l and it is dissociated mainly from plagioclase feldspar at 200 °C. Following the CO_2 injection, the concentration of Na^+ increased from 18001 mg/l to 18411.87 mg/l at the experiment time of 72 h. As explained in Eq. (6), plagioclase feldspar, probably such as albite, releases the Na^+ ion into the brine after CO_2 injection. It is measured as 18473.12 mg/l at the experiment

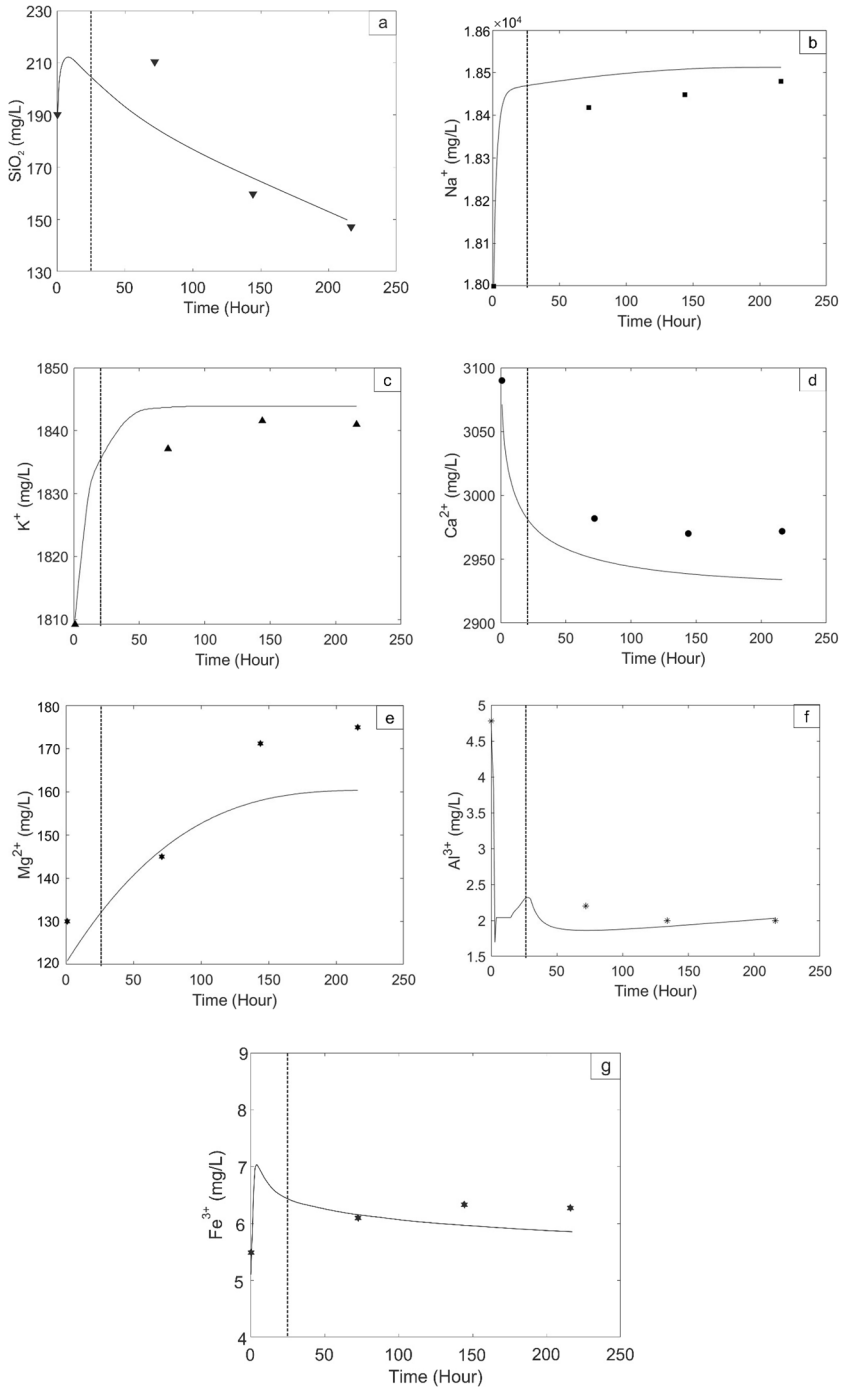


Fig. 6 Evolution of the Tuzla fluid sample after CO_2 injection. The data points explain the measured compositions. The solid lines represent the results of the PhreeqC model, and the vertical dashed lines represent the time of CO_2 injection

time of 216 h. Albite can also form dawsonite, according to Eq. 8, in the presence of CO_2. However, we did not have any significant findings about the precipitation of dawsonite in our experiment. Baker et al. (1995) and Dyni (1997) explain that dawsonite is generally limited to alkaline or highly alkaline environments.

$$NaAlSi_3O_8(Albite) + CO_{2(aq)} + H_2O \leftrightarrow NaAl(CO_3)(OH)_{2(s)}(Dawsonite) + 3SiO_{2(s)} \quad (8)$$

The initial concentration of K^+ 1809.19 mg/l and the origin of K^+ is likely from K-feldspar and/or biotite in the rock sample. The initial brine dissolves the feldspar surface, and K^+ ions leach into the solution. Following the CO_2 injection, the increase in the K^+ concentrations may indicate that the decrease in the pH may cause the dissolution of K-feldspar, releasing the corresponding cations into the brine and generating kaolinite precipitation under the K^+-rich condition (Fig. 6c). Our findings on feldspar behavior are consistent with Fu et al. (2009). Their study stated that feldspar may generate kaolinite in an acidic environment when the temperature reaches 200 °C. The following reaction illustrates these explanations:

$$2KAlSi_3O_8\left(K-feldspar\right) + 2H^+ + 9H_2O \rightarrow 2K^+ + 4H_4SiO_4 + Al_2Si_2O_5(OH)_4(Kaolinite) \quad (9)$$

Dissolution of feldspar is reported in many CO_2 experiments (Chai et al. 2025; Chen et al. 2025; Ding et al. 2025; Fischer et al. 2010; Li et al. 2019; Shiraki and Dunn 2000; Wandrey et al. 2011). Li et al. (2019) stated that the conversion of K-feldspar to kaolinite occurs easily in the conditions of rich Na^+ and at 200 °C. Fu et al. (2009) observed a similar dissolution phenomenon at 200 °C in an acidic environment. Zhu and Lu (2009) explained that boehmite forms in the first stage of albite dissolution. Consistent with the results of Zhu and Lu (2009), we can understand from our experimental results that boehmite was formed during the first 72 h and transformed into kaolinite as albite dissolution continued.

The initial concentration of Ca^{2+} is 3090 mg/l, which comes primarily from anorthite. As a difference from Na^+, the Ca^{2+} concentrations generally decrease during fluid–rock interaction (Fig. 6d). This may indicate the Ca^{2+} has been consumed by either calcite or secondary Ca-aluminosilicates. Another reason might be an increase in temperature. Straub (1932) explained that the solubility of Ca^{2+} is inversely proportional to temperature. The Ca^{2+} concentration decreased to 2971.90 mg/l at the experiment time of 216 h. A general conversion of Ca end-member, anorthite, is explained by Hangx and Spiers (2009) and Oelkers et al. (2008).

$$CaAl_2Si_2O_8(Anorthite) + CO_2 + 2H_2O = CaCO_3(Calcite) + Al_2Si_2O_5(OH)_4(Kaolinite) \quad (10)$$

As anorthite dissolves in acidic brine, the Ca^{2+} is probably consumed by calcite, indicating a tendency towards Eq. 10 governing fluid chemistry (Fig. 6d). On the other hand, the Ca/Na ratios of the brine are consistently low compared to the initial composition (Table 1). The Ca/Na ratio of the brine is initially 0.1717 and decreases to 0.1609 at the experiment time of 216 h. Moreover, the decrease in Ca^{2+} concentration compared to Na^+ and SiO_2 may indicate calcite precipitation on the rock surface. In addition to this, the Ca/Si ratio decreases at the experiment time of 72 h,

which may indicate that calcite precipitation might have occurred. The decrease in the Ca/Si ratio may also indicate that Ca-rich aluminosilicates may also have occurred on the rock sample. The Ca/Si ratio starts to increase after 72 h (Table 1).

Munz et al. (2012) carried out batch reaction experiments at 250 °C with a total pressure of 4 and 12 MPa and found similar observations. They reported that their experimental results showed the conversion of plagioclase feldspar to carbonate was 24–30% at 12 MPa and 11–14% at 4 MPa. A similar observation was reported by Suto et al. (2007). They investigated the initial reactions of a granite sample with a CO_2-injected system over a temperature range of 100–350 °C and at 25 MPa. According to their experiments, injected CO_2 promoted the dissolution of granite and the precipitation of secondary minerals. They found that the solution was supersaturated with respect to calcite at 200 and 300 °C only 6 h after CO_2 injection.

The steep rise in Mg^{2+} concentrations may indicate an ion-exchange process or a fast dissolution, likely from the surface of the mica present (Fig. 6e). The Mg^{2+} is another important divalent cation for carbonate mineralization because releasing the Mg^{2+} into the fluid results in dolomite precipitation on the rock surface (Gislason et al. 2010; Oelkers et al. 2008; Snæbjörnsdóttir et al. 2017). In our experiments, we did not have any findings about the precipitation of dolomite. In contrast, calcite precipitation was the dominant precipitation mechanism among the carbonates. As shown in Table 1, the Mg/Ca ratio increases during the experiment, suggesting a low possibility of dolomite precipitation. Consistent with the Mg/Ca ratio, the Mg^{2+} concentrations increase in the brine.

Initially, the Al^{3+} concentration in the solution is 4.78 mg/l, and it may have originated from Na-endmember albite ($Na[AlSi_3O_8]$) and Ca-endmember anorthite ($Ca[Al_2Si_2O_8)]$ found in plagioclase. The concentration of Al^{3+} decreased sharply to 2.2 mg/l at 72 h and finally decreased to 2 mg/l (Fig. 6f). The decrease in Al^{3+} and Ca^{2+} concentrations after CO_2 injection suggests the possibility of Ca-rich aluminosilicate precipitation.

The Fe^{3+} is probably released from hematite, and the initial concentration of Fe^{3+} is measured as 5.49 mg/l. The reaction between hematite and an acidic environment is given as:

$$Fe_2O_3(Hematite) + 6H^+ \leftrightarrow 2Fe^{3+} + 3H_2O \tag{11}$$

According to Eq. 11, the brine dissolves hematite and releases the Fe^{3+} ion into solution. As seen in Fig. 6g, the Fe^{3+} concentration in the brine increases rapidly after CO_2 injection, indicating the hematite dissolution. It is measured as 6.42 mg/l at the experiment time of 216 h. Here, the Al^{3+} and Fe^{3+} were taken into consideration because aluminum and iron form compounds primarily in the + 3 oxidation state, especially in rock mineral structures.

Since the Cl^- is conservative, it does not present significant changes during the experiment.

Evaluation of reaction progress in fluid chemistry is generally consistent with mineral precipitations in our experiment. Indications from secondary mineral precipitation in our experiment were discussed in the following sections.

Indications from secondary minerals

In this study, we performed a batch reaction experiment on the rock sample under hydrothermal conditions in the presence of brine and CO_2. The experiment was conducted at 200 °C, partial pressure of CO_2 (PCO_2) 2.27 MPa, and total pressure of 4.4 MPa. Tuzla geothermal fluid (11.72 mol NaCl) was chosen to represent reservoir brine. In this experiment, we chose relatively high temperatures to reach Tuzla reservoir conditions and to accelerate mineral reaction rates (Hellmann 1994; Oelkers and

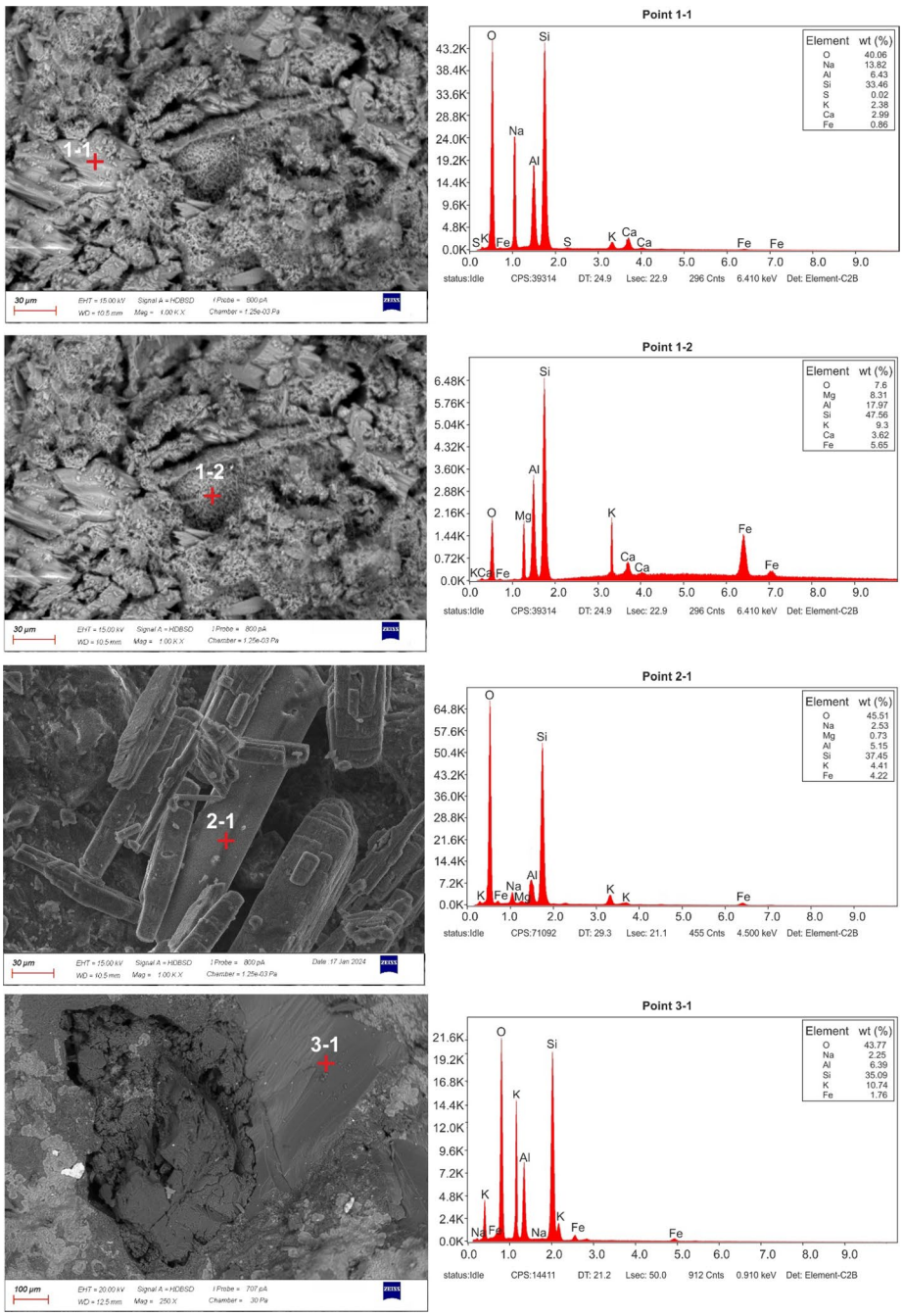


Fig. 7 SEM–EDS results of the rock sample before CO_2 injection

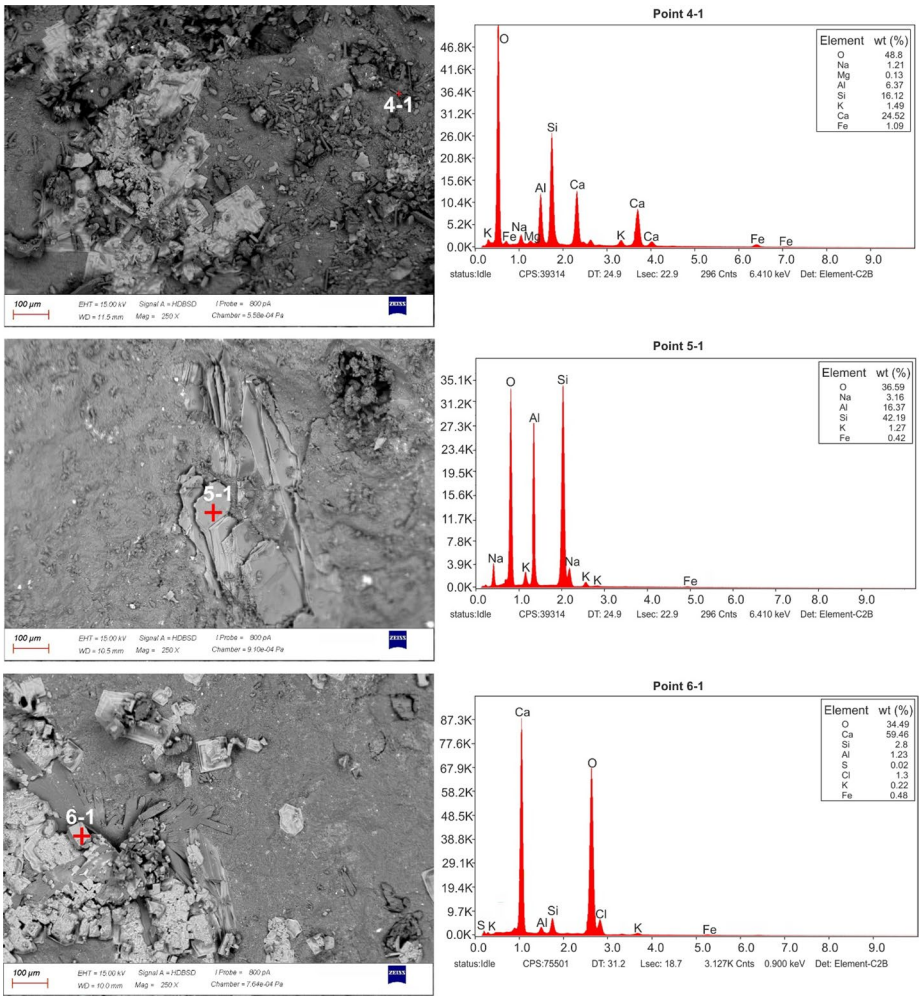


Fig. 8 SEM–EDS results of the rock sample after CO_2 injection

Schott 1995). The rock surface shows significant secondary mineral precipitations after reaction with CO_2 at 200 °C. The images of the fresh sample and these important surface precipitations are given in Figs. 7 and 8.

At point 1–1, the mineral shows adjacent grains with relatively smooth but angular faces. It is clearly distinguishable from the surrounding matrix due to its higher brightness (suggesting it may be more electron-dense or composed of heavier elements), and it has relatively sharp boundaries with adjacent grains, so it may be a plagioclase feldspar. It can be concluded that the mineral is mainly albite ($NaAlSi_3O_8$) because Na, Al, and Si elements exhibit higher peaks than other elements in the EDS (Fig. 7). As seen in Fig. 7, albite is primarily detected in the SEM images. Therefore, the initial Na, Al, and Si elements in the brine may have been derived from primary albite.

At point 1–2, the SEM image shows porous and spongy, with a highly irregular, micro granular surface. The EDS result shows K, Mg, Al, Si, and Fe are relatively high, and the results agree with the mineral at point 1–2 is biotite ($K(Mg,Fe)_3(AlSi_3O_{10})(OH)_2$), which is iron-rich aluminosilicate (Fig. 7).

The mineral at point 2–1 seems typically smooth and subhedral grain. Being of characteristic peaks Si and O, the mineral is the primary quartz on the rock surface, which has a small amount of Fe, Al, and other elements.

At point 3–1, the EDS shows that the O, K, Al, and Si are relatively high compared to other elements. In addition, the mineral has a high peak for K. It is characterized by a smooth, platy to blocky surface in the SEM image. Considering the mineral structure and elemental composition, it can be concluded that the mineral is a feldspar, most likely K-feldspar (Fig. 7).

At point 4–1, the mineral has a needle-shaped appearance. The EDS result of the mineral shows that it has a high elemental composition of Ca, Al, Si, K, and O and contains lower amounts of Mg, Fe, and Na (Fig. 8). All these characterizations suggest that the Ca aluminosilicate mineral may have been precipitated on the rock surface after CO_2 injection. After CO_2 injection, scolecite mineral was detected in the XRD result (Fig. 10b), confirming that the mineral is Ca aluminosilicate.

At point 5–1, according to the EDS result, the mineral has high amounts of O, Al, and Si. In the SEM image, the fact that the mineral appears to fill the spaces and gaps between more structured grains strengthens the possibility that the mineral formed as a secondary mineral after CO_2 injection. This strengthens the possibility that the mineral is probably kaolinite at point 5–1 (Fig. 8). The chemical process behind the formation of kaolinite is the reaction of feldspar and albite with CO_2 to form kaolinite, as explained in Eq. 7 and Eq. 9. The brine reacts with excess K^+ ions in the brine, leading to feldspar formation. At point 5–1, kaolinite forms a booklet-like structure and acts like the primary cementing material. Similar observations were reported in secondary kaolinite formation studies at 200 °C, near-neutral pH and initially acidic pH conditions (Bjørlykke and Aagaard 1992; Ehrenberg 1991; Ehrenberg et al. 1993; Huang et al. 1986). Huang et al. (1986) stated that the conversion of albite to illite mostly occurs under near-neutral pH conditions, while kaolinite forms in an initially acidic solution. Our geochemical model and experimental data indicate that changes in fluid chemistry, such as an increase in Na^+, lead to the conversion of albite to kaolinite, which is consistent with the acidic medium. De Silva et al. (2017) and Othman et al. (2018) stated that kaolinite formation after CO_2 injection can clog small pores and throats, which results in increased reservoir heterogeneity. In another study, Wang et al. (2024) explained that kaolinite formation contributes to pore blockage and decreased permeability, which plays a critical role in CO_2 sequestration.

At point 6–1, the EDS result suggests the mineral is characterized by Ca and O, which is typical for calcite. Additionally, the rhombohedral cleavage shape and a small granular mineral crystallization in its SEM analysis suggest that it is obviously a new mineral formed via chemical reactions. According to Eq. 10, anorthite releases the Ca^{2+} ions in an acidic environment, and they were consumed by calcite at point 6–1. The detection of anorthite in the XRD results is consistent with these reactions (Fig. 10a). In our batch reaction experiments, no magnesite and siderite precipitation were observed except for calcite. The reason for this might be mineral inhabitation, which is due to the solution not reaching the necessary time for nucleation. If enough time were allowed for appropriate ions, such as Ca^{2+} or Al^{3+}, to be released by anorthite or albite breakdown, respectively, it is not implausible that carbonates would eventually precipitate. Kaszuba et al.

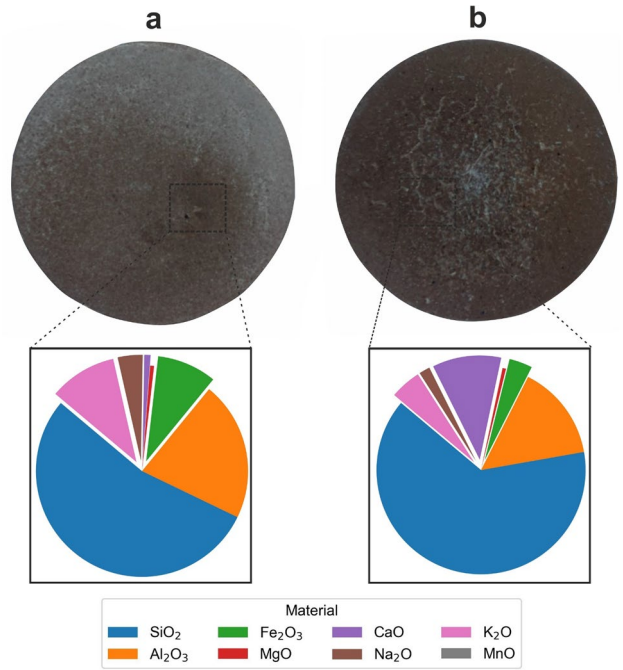


Fig. 9 CO_2 exposure time on the rock surface at different times **a** fresh sample, **b** after CO_2 injection

Table 3 Changes in mineral composition of the rock sample used in this study

Quartz	Plagioclase	Feldspar	Mica	Hematite	Aluminosilicate	Calcite	Kaolinite
Initial mineral content, wt%							
55.7	16.14	11.40	7.62	5.2	4.71	0	0
Mineral content after CO_2 injection, wt%							
63.40	11.91	5.84	4.19	0.9	6.32	5.13	2.33

(2003) conducted a batch experiment over 2.5 months and showed that carbonate precipitation, especially magnesite and siderite, occurred in their experiments at 200 °C and 20 MPa total pressure. In our experiments, calcite was the dominant mineral among carbonates (Fig. 8).

As can be seen in Fig. 9, prior to CO_2 exposure, the rock sample is mainly composed of SiO_2, Al_2O_3, Fe_2O_3, Na_2O, and K_2O. These elemental compositions are related to quartz, plagioclase, K-feldspar, hematite, and biotite (Table 3), which agree with the XRD analysis (Fig. 10a). Figure 9 presents significant evidence for geochemical changes in the rock sample after CO_2 injection. Following CO_2 injection, CaO increased significantly, while K_2O, Na_2O, and Fe_2O_3 decreased (Fig. 9). On the other hand, SiO_2 increased, and Al_2O_3 decreased slightly. The mineral composition was obtained by XRD, and the XRD peak correlations detected are given in Fig. 10. According to Fig. 10a, the rock sample is mainly composed of silicate, feldspar, plagioclase, and hematite, which are in high agreement with the SEM–EDS and mineral compositions (Figs. 7 and 8). After CO_2 injection, the XRD clearly identifies kaolinite, calcite, and scolecite precipitation on the rock surface (Fig. 10b). On one hand, the experimental results presented in Figs. 9 and 10 show a high degree of agreement

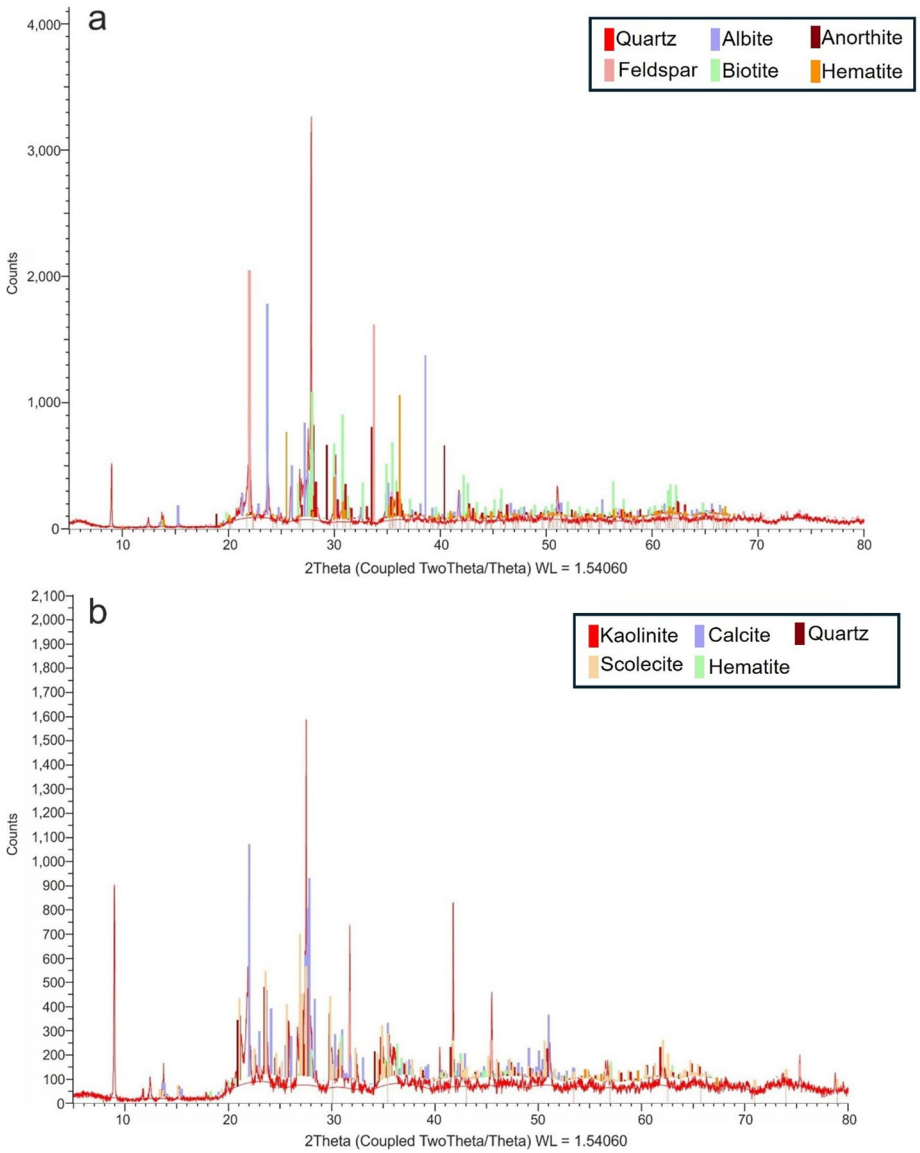


Fig. 10 XRD results of the rock sample, **a** before experiment, **b** after experiment

with the types and concentrations of ions (Fig. 6), and the variations in mineral composition observed in the PhreeqC model (Fig. 11). As shown in Fig. 11, quartz weighed from 55.7 to 63.40%, and aluminosilicates weighed from 4.71 to 6.32%. On the other hand, plagioclase (weight decrease from 16.14 to 11.91%), feldspar (weight decrease from 11.40 to 5.84%), mica (weight decrease from 7.62 to 4.19%), and hematite (weight decrease from 5.2 to 0.9%) all tended to dissolve after CO_2 injection. Moreover, although calcite and kaolinite were not detected in the initial mineral content, they showed a tendency to precipitate after CO_2 injection, exhibiting 5.13% and 2.33% weight, respectively.

In addition, the geochemical modeling findings also revealed secondary minerals (calcite, Ca-aluminosilicates, and kaolinite) that were not detected in the experiment

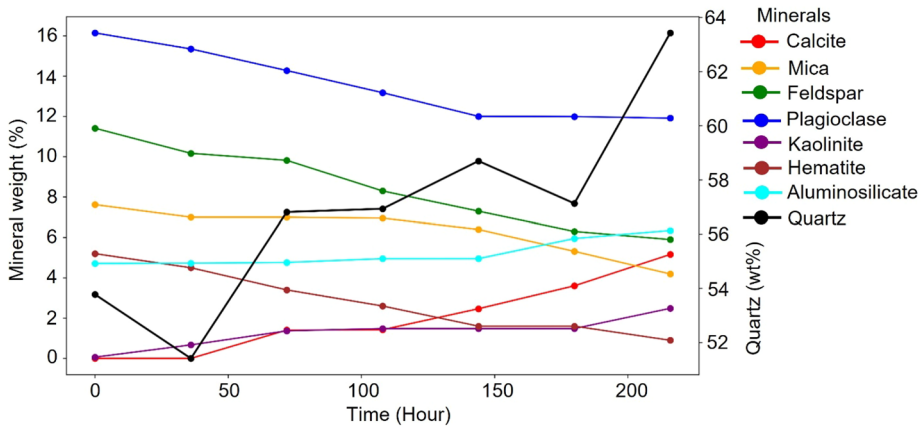


Fig. 11 Mineral content changes with respect to time

before CO_2 injection. These findings provide valuable references for batch reaction experiments utilizing actual brine and for guiding related CO_2 sequestration projects in volcanic fields. On the other hand, this model allows for the exploration of the processes of CO_2–brine–rock interactions in volcanic reservoirs by accounting for variations in mineral composition.

Our geochemical and experimental results showed that if there are sufficient divalent cations in the brine, such as Ca^{2+} and Mg^{2+}, due to the injection of CO_2, they will react with minerals to form carbonates. In our experiments, calcite ($CaCO_3$) was the dominant cation among the carbonates. The total duration of the experiment was 216 h. If the experiment duration had been longer and sufficient cations had been provided for the precipitation of magnesite and siderite, these minerals would probably have been observed in our experiment (Lindeberg et al. 2003). The secondary mineral precipitation in the pore spaces of rocks can decrease porosity and permeability, which may generate a negative effect on reservoir injectivity and stability (Major et al. 2018). Our experimental findings also show the kaolinite formation, one of the secondary minerals. Wang et al. (2024) stated that kaolinite can affect porosity and permeability by acting as cement in the reservoir after CO_2 injection.

In general, our experimental, analytical, and geochemical modeling results are consistent with previous studies that the increased acidity resulting from CO_2 injection into brine and rock samples will dissolve primary feldspars and precipitate calcite, kaolinite, and Ca-aluminosilicate.

Comparison to other studies

Volcanic rocks have the advantage of rapid mineralization due to their high concentration of reactive minerals such as basalt and andesite, which accelerate the reaction of injected CO_2 into stable carbonate minerals. On the contrary, although lower-temperature saline aquifers generally provide very large storage capacities and are more widely distributed geographically, the mineralization process is slower and trapping relies more on structural, residual, and solubility mechanisms. Therefore, volcanic reservoirs may provide a more secure long-term solution due to permanent mineral trapping, whereas saline aquifers remain advantageous in terms of storage volume, availability, and

operational feasibility due to solubility trapping. In other words, while low-temperature saline aquifers offer a more suitable CO_2 storage environment regarding capacity and prevalence, volcanic reservoirs provide a more appropriate environment regarding efficiency and sustainability.

The interaction of CO_2–brine–minerals has been the subject of experimental studies reported by several researchers (Bischoff and Rosenbauer 1996; Ding et al. 2025; Lagache 1965, 1976; Suto et al. 2007). The chemical reactions of feldspar under CO_2 via batch experiments were studied by Hangx and Spiers (2009). They injected CO_2 into the reactor at 200–300 °C and 0.4–15 MPa, and kaolinite and smectite/illite formed in their studies. Hangx and Spiers (2009) concluded that kaolinite precipitation can proceed or accompany carbonate precipitation in these conditions. Shiraki and Dunn (2000) studied mineral dissolution and precipitation during CO_2 injection in northern Wyoming, USA. They conducted the batch reaction experiment under reservoir conditions, which are 80 °C and 16.6 MPa. Their results concluded that the major reaction was the dissolution of K-feldspar to form kaolinite. Lagache (1965) used albite, adularia, and labradorite in a series of feldspar alteration studies at 100, 150, and 200 °C with and without CO_2. Lagache (1965) stated that when the solution was saturated with silica, the feldspars changed into boehmite, kaolinite, and mica (muscovite), and the rate of dissolution was a function of the activity ratio of Na^+ or K^+ to H^+. However, in our study, there is no strong evidence for the precipitation of boehmite as a secondary formation. Ding et al. (2025) investigated the geochemical changes in CO_2–fluid–rock interaction under high temperature and high pressure. After the CO_2 injection, they observed that K-feldspar decreased from 9 to 4.1 wt% by weight, plagioclase decreased from 22.3 to 12 wt%, quartz increased from 56.6 to 70.2 wt%, and calcite increased from 5.5 to 6.1 wt%. Our results in Fig. 11 are in good agreement with similar studies (Ding et al. 2025; Suto et al. 2007; Yu et al. 2012; Zhang et al. 2018). The effect of CO_2 injection into the reactor with a granite sample on the enhanced geothermal system (EGS) at 20 MPa and 300 °C using a high-temperature oil bath was studied by Li et al. (2023). After CO_2 injection, they concluded that the minerals dissolved in the granite sample were mainly feldspars, especially albite and K-feldspar. In addition to these, they observed the newly formed minerals such as calcite and aluminosilicates on the granite sample. The SEM results in our experiments agree favorably with the study of Li et al. (2023) on the granite sample treated with CO_2 at 100–300 °C and in the presence of geothermal fluid. On the other hand, our experiment results and fluid chemistry strongly agree with those of Suto et al. (2007). They conducted a batch reaction experiment with CO_2 at 100–350 °C and 0–25 MPa and concluded that kaolinite, calcite, smectite, and muscovite precipitated as secondary phases.

Uncertainties and limitations of kinetic reaction path modeling

As can be seen, mineral dissolution and precipitation processes are extremely complex reactions. Thus, it is not possible to completely simulate these kinds of reactions due to differences in temperature and pH conditions, and ion-exchange reactions (Ganor et al. 2007). There are many unknowns in geochemical modeling, especially when dealing with sophisticated multiphase systems. These kinetic calculations depend on the

experimentally established dissolution rate data in addition to a thorough and reliable thermodynamic database.

Although the time history of dissolution reactions may be adequately described by these rate data, their application to the modeling of precipitation processes has produced inconsistent results when compared to laboratory and natural observations (Schott et al. 2009). Accurate modeling of the temporal evolution of natural water–rock systems is commonly hindered by the lack of established data for the majority of these systems due to the decline in chemical affinity and reaction rates as equilibrium approaches. The impact of different mineral compositions in solid solution series and the nonideal mineral crystallinity also hamper an evaluation with the geochemical modeling. For this reason, sometimes calculated and measured rates typically differ by several orders of magnitude when creating a consistent mineral dissolution database. Our kinetic rate constants for plagioclase feldspar were higher than those obtained by Fu et al. (2009), which is probably due to the salinity effect (England 1990). In addition, the kinetic rates in our experiment obtained one order of magnitude more than those from Snæbjörnsdóttir et al. (2018). The reason is probably the pH difference used in this study. Snæbjörnsdóttir et al. (2018) investigated CO_2 sequestration potential in the Hellisheidi volcanic reservoir with pH 9.5 in Iceland at the CarbFix project site.

A large portion of this uncertainty can be eliminated by acquiring detailed and precise physical and chemical characteristics particular to the system and/or place, as was done in the current work. Indeed, in the absence of convective flow, the contact between CO_2 and the reservoir rock becomes limited, and the injected CO_2 may preferentially accumulate in the upper parts of the reservoir. Additionally, the solubility of CO_2 decreases significantly with increasing NaCl concentration, which further restricts its distribution in the brine. A detailed investigation of CO_2 transport dynamics under such conditions is, however, beyond the scope of the present study.

Despite all these uncertainties and limitations, the geochemical computation programs working on the law of mass action such as the PhreeqC provide straightforward evaluation in such intricate reservoir systems including multi-oxides and high salinity.

In addition, the use of powdered rock in batch reactors provides high surface area and thus accelerates dissolution and precipitation reactions, allowing the identification of reactive mineral phases under controlled conditions. However, unlike reactive core-flooding experiments, batch experiments do not account for flow, transport, or pore geometry, and therefore, the results obtained in this study should be interpreted as indicators of mineral reactivity. While these experiments provide valuable insights into mineral reactivity, we acknowledge that uncertainties remain due to experimental simplifications, and although the observed trends are reproducible under the applied conditions, absolute reaction rates may vary in natural systems.

Conclusions

The TGF is the first pilot site in Türkiye where the CO_2 co-injection study was carried out. Currently, the CO_2 co-injection study at TGF is continuing successfully, and the scaling problem in the wellbores and surface installations has decreased significantly. In this study, a batch reaction experiment and geochemical modeling were performed to analyze rock–fluid–CO_2 interactions for insights into the CO_2 sequestration potential

and challenges in a volcanic reservoir. The experimental results, which were conducted at 200 °C and 4.4 MPa, showed that the initial reaction of the rock sample is characterized by the dissolution of plagioclase feldspar. After CO_2 injection, the rock sample tended to form calcite, kaolinite, and Ca-rich aluminosilicate as secondary minerals; that is, the rock sample might have the potential to capture CO_2 under reservoir conditions. The formation of calcite as a secondary mineral after CO_2 injection is important for carbonation, which means that the TGF is a suitable site for CO_2 sequestration at 200 °C and 4.4 MPa. Based on this, the TGF may be a potential geothermal field for CO_2 sequestration in the future, and these study findings can lead to the development of the current system used in the TGF. Therefore, our results show the CO_2 co-injection study currently used in TGF can be extended to CO_2 sequestration in the future, capturing the CO_2 of the system itself released during the production.

Acknowledgements
The authors are thankful to the two anonymous reviewers for their constructive comments and suggestions, which greatly improved the quality of this manuscript. We would like to thank the staff of Tuzla Geothermal Company., who supported the field work at every stage of the project.

Author contributions
Serhat Tonkul: Original draft, numerical modeling, experimental design, investigation, Selçuk Erol: Investigation, methodology, Alper Baba: reviewing and editing, Simona Regenspurg: paper review and revision.

Funding
This study received funding from the European Union's Horizon 2020 research and innovation programme under grant agreement No. 850626 (REFLECT). We also thank the Scientific and Technological Research Council of Türkiye (TÜBİTAK) TÜBİTAK 2214-A International Research Fellowship Programme for funding this study.

Data availability
No datasets were generated or analysed during the current study.

Declarations

Ethics approval and consent to participate
Not applicable.

Consent for publication
Not applicable.

Competing interests
The authors declare no competing interests.

Received: 15 June 2025 Accepted: 24 December 2025
Published online: 22 January 2026

References

Aagaard P, Helgeson HC. Thermodynamic and kinetic constraints on reaction rates among minerals and aqueous solutions; I, Theoretical considerations. Am J Sci. 1982;282(3):237–85. https://doi.org/10.2475/ajs.282.3.237.

Addassi M, Omar A, Hoteit H, Afifi AM, Arkadakskiy S, Ahmed ZT, et al. Assessing the potential of solubility trapping in unconfined aquifers for subsurface carbon storage. Sci Rep. 2022;12(1):20452. https://doi.org/10.1038/s41598-022-24623-6.

Ajayi T, Gomes JS, Bera A. A review of CO_2 storage in geological formations emphasizing modeling, monitoring and capacity estimation approaches. Pet Sci. 2019;16:1028–63. https://doi.org/10.1007/s12182-019-0340-8.

Akın T, Erol S, Tokel AB, Sevindik DB, Akın S. Monitoring CO_2 injection in the Kızıldere geothermal field. Int J Greenh Gas Control. 2025;146:104413. https://doi.org/10.1016/j.ijggc.2025.104413.

Anbeek C. Surface roughness of minerals and implications for dissolution studies. Geochim Cosmochim Acta. 1992;56(4):1461–9. https://doi.org/10.1016/0016-7037(92)90216-6.

Aradóttir E, Sonnenthal E, Björnsson G, Jónsson H. Multidimensional reactive transport modeling of CO_2 mineral sequestration in basalts at the Hellisheidi geothermal field, Iceland. Int J Greenh Gas Control. 2012;9:24–40. https://doi.org/10.1016/j.ijggc.2012.02.006.

Bachu S, Bonijoly D, Bradshaw J, Burruss R, Holloway S, Christensen NP, et al. CO_2 storage capacity estimation: methodology and gaps. Int J Greenh Gas Control. 2007;1(4):430–43. https://doi.org/10.1016/S1750-5836(07)00086-2.

Baker JC, Bai GP, Hamilton PJ, Golding SD, Keene JB. Continental-scale magmatic carbon dioxide seepage recorded by dawsonite in the Bowen-Gunnedah-Sydney Basin system, eastern Australia. J Sediment Res. 1995;65(3a):522–30. https://doi.org/10.1306/d4268117-2b26-11d7-8648000102c1865d.
Beckingham LE, Mitnick EH, Steefel CI, Zhang S, Voltolini M, Swift AM, et al. Evaluation of mineral-reactive surface area estimates for prediction of reactivity of a multi-mineral sediment. Geochim Cosmochim Acta. 2016;188:310–29. https://doi.org/10.1016/j.gca.2016.05.040.
Berndsen M, Erol S, Akın T, Akın S, Nardini I, Immenhauser A, et al. Experimental study and kinetic modeling of high temperature and pressure CO_2 mineralization. Int J Greenh Gas Control. 2024;132:104044. https://doi.org/10.1016/j.ijggc.2023.104044.
Bischoff JL, Rosenbauer RJ. The alteration of rhyolite in CO_2 charged water at 200 and 350 C: the unreactivity of CO_2 at higher temperature. Geochim Cosmochim Acta. 1996;60(20):3859–67. https://doi.org/10.1016/0016-7037(96)00208-6.
Bjørlykke K, Aagaard P. Clay minerals in North Sea sandstones. Claremore: SEPM Special Publication; 1992.
Brunauer S, Emmett PH, Teller E. Adsorption of gases in multimolecular layers. J Am Chem Soc. 1938;60(2):309–19.
Burch T, Nagy K, Lasaga A. Free energy dependence of albite dissolution kinetics at 80 C and pH 8.8. Chem Geol. 1993;105(1–3):137–62. https://doi.org/10.1016/0009-2541(93)90123-Z.
Chai R, Ma Q, Goodarzi S, Yow FY, Bijeljic B, Blunt MJ. Multiphase reactive flow during CO_2 storage in sandstone. Engineering. 2025. https://doi.org/10.1016/j.eng.2025.01.016.
Chen F, Yang L, Hu Q, Wang L, Bai Y, Gu J. Experimental study of CO_2 flow behavior and storage potential within low porosity and permeability aquifer. J CO2 Util. 2025;92:103027. https://doi.org/10.1016/j.jcou.2025.103027.
Clark DE, Oelkers EH, Gunnarsson I, Sigfússon B, Snæbjörnsdóttir SÓ, Aradottir ES, et al. CarbFix2: CO2 and H2S mineralization during 3.5 years of continuous injection into basaltic rocks at more than 250 C. Geochimica et Cosmochimica Acta. 2020;279:45–66. https://doi.org/10.1016/j.gca.2020.03.039.
De Silva G, Ranjith P, Perera M, Dai Z, Yang S. An experimental evaluation of unique CO_2 flow behaviour in loosely held fine particles rich sandstone under deep reservoir conditions and influencing factors. Energy. 2017;119:121–37. https://doi.org/10.1016/j.energy.2016.11.144.
Dethlefsen F, Haase C, Ebert M, Dahmke A. Uncertainties of geochemical modeling during CO_2 sequestration applying batch equilibrium calculations. Environ Earth Sci. 2012;65:1105–17. https://doi.org/10.1007/s12665-011-1360-x.
Ding W, Jiang T, Chen W, Hu D, Zhou H, Yang F. Experimental study on CO_2–brine–sandstone interaction and reservoir stability analysis under high temperature and high pressure. Renew Energy. 2025. https://doi.org/10.1016/j.renene.2025.123146.
Dyni, J. R. (1997). Sodium carbonate resources of the Green River Formation. Reston, VA, USA: US Geological Survey. Karamanderesi, İ.H., 1986. Hydrothermal alteration in well Tuzla T-2, Çanakkale, Turkey. UNU Geothermal Training Prog. Report, 3,36. Reykjavik.
Ehrenberg S. Kaolinized, potassium-leached zones at the contacts of the Garn Formation, Haltenbanken, mid-Norwegian continental shelf. Mar Pet Geol. 1991;8(3):250–69. https://doi.org/10.1016/0264-8172(91)90080-K.
Ehrenberg S, Aagaard P, Wilson M, Fraser A, Duthie D. Depth-dependent transformation of kaolinite to dickite in sandstones of the Norwegian continental shelf. Clay Miner. 1993;28(3):325–52. https://doi.org/10.1180/claymin.1993.028.3.01.
England W. The organic geochemistry of petroleum reservoirs. Org Geochem. 1990;16(1–3):415–25. https://doi.org/10.1016/0146-6380(90)90058-8.
Erol S, Akın T, Başer A, Saraçoğlu Ö, Akın S. Fluid–CO_2 injection impact in a geothermal reservoir: evaluation with 3-D reactive transport modeling. Geothermics. 2022;98:102271. https://doi.org/10.1016/j.geothermics.2021.102271.
Fawzy S, Osman AI, Doran J, Rooney DW. Strategies for mitigation of climate change: a review. Environ Chem Lett. 2020;18:2069–94. https://doi.org/10.1007/s10311-020-01059-w.
Fischer S, Liebscher A, Wandrey M, Group CS. CO2–brine–rock interaction—First results of long-term exposure experiments at in situ P-T conditions of the Ketzin CO2 reservoir. Geochemistry. 2010;70:155–64. https://doi.org/10.1016/j.chemer.2010.06.001.
Fu Q, Lu P, Konishi H, Dilmore R, Xu H, Seyfried W Jr, et al. Coupled alkali-feldspar dissolution and secondary mineral precipitation in batch systems: 1. New experiments at 200 C and 300 bars. Chem Geol. 2009;258(3–4):125–35.
Galeczka IM, Stefánsson A, Kleine BI, Gunnarsson-Robin J, Snæbjörnsdóttir SÓ, Sigfússon B, et al. A pre-injection assessment of CO_2 and H_2S mineralization reactions at the Nesjavellir (Iceland) geothermal storage site. Int J Greenh Gas Control. 2022;115:103610. https://doi.org/10.1016/j.ijggc.2022.103610.
Ganor J, Lu P, Zheng Z, Zhu C. Bridging the gap between laboratory measurements and field estimations of silicate weathering using simple calculations. Environ Geol. 2007;53:599–610. https://doi.org/10.1007/s00254-007-0675-0.
Gautier JM, Oelkers EH, Schott J. Experimental study of K-feldspar dissolution rates as a function of chemical affinity at 150 C and pH 9. Geochim Cosmochim Acta. 1994;58(21):4549–60. https://doi.org/10.1016/0016-7037(94)90190-2.
Gislason SR, Wolff-Boenisch D, Stefansson A, Oelkers EH, Gunnlaugsson E, Sigurdardottir H, et al. Mineral sequestration of carbon dioxide in basalt: a pre-injection overview of the CarbFix project. Int J Greenhouse Gas Control. 2010;4(3):537–45. https://doi.org/10.1016/j.ijggc.2009.11.013.
Haase C, Ebert M, Dethlefsen F. Uncertainties of geochemical codes and thermodynamic databases for predicting the impact of carbon dioxide on geologic formations. Appl Geochem. 2016;67:81–92. https://doi.org/10.1016/j.apgeochem.2016.01.008.
Hangx SJ, Spiers CJ. Reaction of plagioclase feldspars with CO_2 under hydrothermal conditions. Chem Geol. 2009;265(1–2):88–98. https://doi.org/10.1016/j.chemgeo.2008.12.005.
Hellmann R. The albite–water system: Part I. The kinetics of dissolution as a function of pH at 100, 200 and 300 C. Geochimica et Cosmochimica Acta. 1994;58(2):595–611. https://doi.org/10.1016/0016-7037(94)90491-X.
Heřmanská M, Kleine BI, Stefánsson A. Geochemical constraints on supercritical fluids in geothermal systems. J Volcanol Geotherm Res. 2020;394:106824. https://doi.org/10.1016/j.jvolgeores.2020.106824.

Hodson ME. Micropore surface area variation with grain size in unweathered alkali feldspars: implications for surface roughness and dissolution studies. Geochim Cosmochim Acta. 1998;62(21–22):3429–35. https://doi.org/10.1016/S0016-7037(98)00244-0.
Holdren GR Jr, Speyer PM. Reaction rate-surface area relationships during the early stages of weathering. II. Data on eight additional feldspars. Geochimica et Cosmochimica Acta. 1987;51(9):2311–8. https://doi.org/10.1016/0016-7037(87)90284-5.
Huang W, Bishop A, Brown R. The effect of fluid/rock ratio on feldspar dissolution and illite formation under reservoir conditions. Clay Miner. 1986;21(4):585–601. https://doi.org/10.1180/claymin.1986.021.4.10.
Junior GS, Castro-Gomes J, Magrinho M. Carbon capture and utilisation technologies: A systematic analysis of innovative applications and supercritical CO_2 viability strategies. J CO2 Util. 2025;97:103115. https://doi.org/10.1016/j.jcou.2025.103115.
Karamanderesi IH. Hydrothermal alteration in well Tuzla T-2, Canakkale, Turkey; 1986.
Kaszuba JP, Janecky DR, Snow MG. Carbon dioxide reaction processes in a model brine aquifer at 200 C and 200 bars: implications for geologic sequestration of carbon. Appl Geochem. 2003;18(7):1065–80. https://doi.org/10.1016/S0883-2927(02)00239-1.
Kaya E, Zarrouk SJ. Reinjection of greenhouse gases into geothermal reservoirs. Int J Greenh Gas Control. 2017;67:111–29. https://doi.org/10.1016/j.ijggc.2017.10.015.
Kieffer B, Jové CF, Oelkers EH, Schott J. An experimental study of the reactive surface area of the Fontainebleau sandstone as a function of porosity, permeability, and fluid flow rate. Geochim Cosmochim Acta. 1999;63(21):3525–34. https://doi.org/10.1016/S0016-7037(99)00191-X.
Kolditz O, Bauer S, Beyer C, Böttcher N, Dietrich P, Görke U-J, et al. A systematic benchmarking approach for geologic CO_2 injection and storage. Environ Earth Sci. 2012;67(2):613–32. https://doi.org/10.1007/s12665-012-1656-5.
Lagache M. Contribution à l'étude de l'altération des feldspaths, dans l'eau entre 100 et 200° C, sous diverses pressions de CO_2 et application à la synthèse des minéraux argileux. Bull Minér. 1965;88(2):223–53.
Lagache M. New data on the kinetics of the dissolution of alkali feldspars at 200 C in CO_2 charged water. Geochim Cosmochim Acta. 1976;40(2):157–61. https://doi.org/10.1016/0016-7037(76)90173-3.
Lasaga A. C. (1981) Transition state theory. In: Lasaga A. C. and Kirkpatrick R. J. (ed) Kinetics of Geochemical Processes. RevMineral 8. Mineral Society of America, Washington DC, pp. 135-170.
Li L, Salehikhoo F, Brantley SL, Heidari P. Spatial zonation limits magnesite dissolution in porous media. Geochim Cosmochim Acta. 2014;126:555–73. https://doi.org/10.1016/j.gca.2013.10.051.
Li M, Li C, Xing J, Sun X, Yuan G, Cao Y. An experimental study on dynamic coupling process of alkaline feldspar dissolution and secondary mineral precipitation. Acta Geochim. 2019;38:872–82. https://doi.org/10.1007/s11631-019-00326-0.
Li P, Hao Y, Wu Y, Wanniarachchi A, Zhang H, Cui Z. Experimental study on the effect of CO_2 storage on the reservoir permeability in a CO_2-based enhanced geothermal system. Geotherm Energy. 2023;11(1):24. https://doi.org/10.1186/s40517-023-00266-2.
Lichtner P, Carey J, O'Connor W, Dahlin D, Guthrie Jr G. Geochemical mechanisms and models of olivine carbonation, Proceedings of the 28th International Technical Conference on Coal Utilization & Fuel Systems; 2003.
Lindeberg E, Bergmo P, Moen A. The long-term fate of CO_2 injected into an aquifer. Greenh Gas Control Technol. 2003;1:489–94.
Liu B, Zhao F, Xu J, Qi Y. Experimental investigation and numerical simulation of CO_2–brine–rock interactions during CO_2 sequestration in a deep saline aquifer. Sustainability. 2019;11(2):317. https://doi.org/10.3390/su11020317.
Lu P, Konishi H, Oelkers E, Zhu C. Coupled alkali feldspar dissolution and secondary mineral precipitation in batch systems: 5. Results of K-feldspar hydrolysis experiments. Chin J Geochem. 2015;34:1–12. https://doi.org/10.1007/s11631-014-0029-z.
Luhmann AJ, Kong X-Z, Tutolo BM, Garapati N, Bagley BC, Saar MO, et al. Experimental dissolution of dolomite by CO_2-charged brine at 100 C and 150 bar: evolution of porosity, permeability, and reactive surface area. Chem Geol. 2014;380:145–60. https://doi.org/10.1016/j.chemgeo.2014.05.001.
Luo X, Yang W, Li R, Gao L. Effects of pH on the solubility of the feldspar and the development of secondary porosity. Bull Miner Petrol Geochem. 2001;20:103–7.
Luo S, Xu R, Jiang P. Effect of reactive surface area of minerals on mineralization trapping of CO_2 in saline aquifers. Pet Sci. 2012;9:400–7.
Major JR, Eichhubl P, Dewers TA, Olson JE. Effect of CO_2–brine–rock interaction on fracture mechanical properties of CO_2 reservoirs and seals. Earth Planet Sci Lett. 2018;499:37–47. https://doi.org/10.1016/j.epsl.2018.07.013.
Matter JM, Stute M, Snæbjörnsdottir SÓ, Oelkers EH, Gislason SR, Aradottir ES, et al. Rapid carbon mineralization for permanent disposal of anthropogenic carbon dioxide emissions. Science. 2016;352(6291):1312–4. https://doi.org/10.1126/science.aad8132.
Munz IA, Brandvoll Ø, Haug T, Iden K, Smeets R, Kihle J, et al. Mechanisms and rates of plagioclase carbonation reactions. Geochim Cosmochim Acta. 2012;77:27–51. https://doi.org/10.1016/j.gca.2011.10.036.
Mützenberg SR. Westliche Biga-Halbinsel (Canakkale, Türkei): Beziehung zwischen geologie, tektonik und entwicklung der thermalquellen. ETH Zurich; 1990.
Nagy K, Lasaga A. Dissolution and precipitation kinetics of gibbsite at 80 C and pH 3: the dependence on solution saturation state. Geochim Cosmochim Acta. 1992;56(8):3093–111. https://doi.org/10.1016/0016-7037(92)90291-P.
Oelkers EH, Schott J. Experimental study of anorthite dissolution and the relative mechanism of feldspar hydrolysis. Geochim Cosmochim Acta. 1995;59(24):5039–53. https://doi.org/10.1016/0016-7037(95)00326-6.
Oelkers EH, Schott J, Devidal JL. The effect of aluminum, pH, and chemical affinity on the rates of aluminosilicate dissolution reactions. Geochim Cosmochim Acta. 1994;58(9):2011–24. https://doi.org/10.1016/0016-7037(94)90281-X.
Oelkers EH, Gislason SR, Matter J. Mineral carbonation of CO_2. Elements. 2008;4(5):333–7. https://doi.org/10.2113/gselements.4.5.333.
Othman F, Yu M, Kamali F, Hussain F. Fines migration during supercritical CO_2 injection in sandstone. J Nat Gas Sci Eng. 2018;56:344–57. https://doi.org/10.1016/j.jngse.2018.06.001.

Palandri JL, Kharaka YK. A compilation of rate parameters of water-mineral interaction kinetics for application to geochemical modelling. 2004. https://doi.org/10.3133/ofr20041068.
Parkhurst DL, Appelo, C. User's guide to PHREEQC (Version 2): a computer program for speciation, batch-reaction, one-dimensional transport, and inverse geochemical calculations. US Geological Survey. 1999. https://doi.org/10.3133/wri994259.
Přikryl J, Marieni C, Gudbrandsson S, Aradóttir ES, Gunnarsson I, Stefánsson A. H_2S sequestration process and sustainability in geothermal systems. Geothermics. 2018;71:156–66. https://doi.org/10.1016/j.geothermics.2017.09.010.
Saadatpoor E, Bryant SL, Sepehrnoori K. New trapping mechanism in carbon sequestration. Transp Porous Media. 2010;82(1):3–17. https://doi.org/10.1007/s11242-009-9446-6.
Samilgil E. Hydrogeological report of geothermal energy possibility survey of hot springs of Kestanbol and Tuzla village of Canakkale. MTA report 4274; 1966.
Schott J, Pokrovsky OS, Oelkers EH. The link between mineral dissolution/precipitation kinetics and solution chemistry. Rev Mineral Geochem. 2009;70(1):207–58. https://doi.org/10.2138/rmg.2009.70.6.
Şener M, Gevrek AI. Distribution and significance of hydrothermal alteration minerals in the Tuzla hydrothermal system, Canakkale, Turkey. J Volcanol Geotherm Res. 2000;96(3–4):215–28. https://doi.org/10.1016/S0377-0273(99)00152-3.
Shiraki R, Dunn TL. Experimental study on water–rock interactions during CO_2 flooding in the Tensleep Formation, Wyoming, USA. Appl Geochem. 2000;15(3):265–79. https://doi.org/10.1016/S0883-2927(99)00048-7.
Snæbjörnsdóttir SÓ, Wiese F, Fridriksson T, Ármansson H, Einarsson GM, Gislason SR. CO_2 storage potential of basaltic rocks in Iceland and the oceanic ridges. Energy Proc. 2014;63:4585–600. https://doi.org/10.1016/j.egypro.2014.11.491.
Snæbjörnsdóttir SÓ, Oelkers EH, Mesfin K, Aradóttir ES, Dideriksen K, Gunnarsson I, et al. The chemistry and saturation states of subsurface fluids during the in situ mineralisation of CO_2 and H_2S at the CarbFix site in SW-Iceland. Int J Greenh Gas Control. 2017;58:87–102. https://doi.org/10.1016/j.ijggc.2017.01.007.
Snæbjörnsdóttir SÓ, Gislason SR, Galeczka IM, Oelkers EH. Reaction path modelling of in-situ mineralisation of CO_2 at the CarbFix site at Hellisheidi, SW-Iceland. Geochim Cosmochim Acta. 2018;220:348–66. https://doi.org/10.1016/j.gca.2017.09.053.
Steefel CI, Appelo CAJ, Arora B, Jacques D, Kalbacher T, Kolditz O, et al. Reactive transport codes for subsurface environmental simulation. Comput Geosci. 2015;19:445–78. https://doi.org/10.1007/s10596-014-9443-x.
Steel L, Mackay E, Maroto-Valer MM. Experimental investigation of CO_2-brine-calcite interactions under reservoir conditions. Fuel Process Technol. 2018;169:122–31. https://doi.org/10.1016/j.fuproc.2017.09.028.
Straub FG. Solubility of calcium sulfate and calcium carbonate at temperatures between 1820c and 3160c. Ind Eng Chem. 1932;24(8):914–7.
Suto Y, Liu L, Yamasaki N, Hashida T. Initial behavior of granite in response to injection of CO2-saturated fluid. Appl Geochem. 2007;22(1):202–18. https://doi.org/10.1016/j.apgeochem.2006.09.005.
Tödheide K, Franck E. Das Zweiphasengebiet und die kritische Kurve im System Kohlendioxid–Wasser bis zu Drucken von 3500 bar. Z Phys Chem. 1963;37(5_6):387–401.
Topcu G, Koç GA, Baba A, Demir MM. The injection of CO_2 to hypersaline geothermal brine: a case study for Tuzla region. Geothermics. 2019;80:86–91. https://doi.org/10.1016/j.geothermics.2019.02.01.
Wan Y, Xu T, Song T. Numerical Study on CO_2–Brine–Rock Interaction of Enhanced Geothermal Systems with CO2 as Heat Transmission Fluid, MATEC Web of Conferences. EDP Sciences. 2016; 06010. https://doi.org/10.1051/matecconf/20166706010.
Wandrey M, Fischer S, Zemke K, Liebscher A, Scherf AK, Vieth-Hillebrand A, et al. Monitoring petrophysical, mineralogical, geochemical and microbiological effects of CO_2 exposure—results of long-term experiments under in situ conditions. Energy Proc. 2011;4:3644–50. https://doi.org/10.1016/j.egypro.2011.02.295.
Wang X, Yang H, Huang Y, Liang Q, Liu J, Ye D. Evolution of CO_2 storage mechanisms in low-permeability tight sandstone reservoirs. Engineering. 2024. https://doi.org/10.1016/j.eng.2024.05.013.
White AF, Peterson ML. Role of reactive-surface-area characterization in geochemical kinetic models. Washington, D.C.: ACS Publications; 1990.
Wild B, Daval D, Guyot F, Knauss KG, Pollet-Villard M, Imfeld G. pH-dependent control of feldspar dissolution rate by altered surface layers. Chem Geol. 2016;442:148–59. https://doi.org/10.1016/j.chemgeo.2016.08.035.
Wolery TJ, Daveler SA. EQ6, a computer program for reaction path modeling of aqueous geochemical systems: Theoretical manual, users guide, and related documentation (Version 7.0); Part 4. Lawrence Livermore National Lab.(LLNL), Livermore, CA (United States). 1992. https://doi.org/10.2172/138820.
Yu Z, Liu L, Yang S, Li S, Yang Y. An experimental study of CO_2–brine–rock interaction at in situ pressure–temperature reservoir conditions. Chem Geol. 2012;326:88–101. https://doi.org/10.1016/j.chemgeo.2012.07.030.
Zhang X, Wei B, Shang J, Gao K, Pu W, Xu X, et al. Alterations of geochemical properties of a tight sandstone reservoir caused by supercritical CO_2–brine–rock interactions in CO_2-EOR and geosequestration. J CO2 Util. 2018;28:408–18. https://doi.org/10.1016/j.jcou.2018.11.002.
Zhu C, Lu P. Alkali feldspar dissolution and secondary mineral precipitation in batch systems: 3. saturation states of product minerals and reaction paths. Geochim Cosmochim Acta. 2009;73(11):3171–200. https://doi.org/10.1007/s11631-014-0029-z.

Publisher's Note

Springer Nature remains neutral with regard to jurisdictional claims in published maps and institutional affiliations.